Pure Appl. Chem., ASAP Article
doi:10.1351/PAC-CON-10-11-12

Dendron-functionalized multiwalled carbon nanotubes incorporating polyoxometalates for water-splitting catalysis*

Francesca Maria Toma[1], Andrea Sartorel[2], Mauro Carraro[2], Marcella Bonchio[2], and Maurizio Prato[1,‡]

[1]Center of Excellence for Nanostructured Materials (CENMAT), INSTM, Department of Pharmaceutical Science, University of Trieste, Piazzale Europa 1, 34127 Trieste, Italy; [2]ITM-CNR and Department of Chemical Science, University of Padova, via Marzolo 1, 35131 Padova, Italy

Abstract: Carbon nanotubes (CNTs) are versatile nanomaterials with applications spanning from medicinal chemistry and biology, to electronics as field effect transistors or energy as fuel cells. The major drawback stems from the CNT insolubility in most of the organic and aqueous media, which severely hampers the material processability. To overcome this problem, functionalization of CNTs is generally accomplished by either covalent strategies resulting in the modification of the CNT backbone via radical reactions, fluorination, and/or cycloaddition reactions, or noncovalent protocols, exploiting multiple weak interactions (hydrophobic, van der Waals, electrostatic) with suitable reagents. Herein, we highlight that a rewarding approach includes a combination of covalent/noncovalent methods, by a tailored synthetic modification of the CNT surface with polycationic dendrimeric chains, fostering the successive decoration with a multimetallic and polyanionic water oxidation catalyst. The outcome is a hybrid nanomaterial with unperturbed CNT electrical properties, in close contact with a unique multi-electron catalyst enabling electrocatalytic water splitting with high efficiency at low overpotentials.

Keywords: carbon nanotubes; dendrimers; renewable energy; polyoxometalates; hydrogen production.

INTRODUCTION

Carbon nanotube (CNT) synthesis is plagued by side-contaminations. Indeed, metal nanoparticles and amorphous carbon (AC) are present as residues, and CNTs need to be processed to remove impurities. To address this issue, functionalization approaches provide a key step for manipulation and further application of this material. In general, CNTs are a fluffy powder that is difficult to handle, while chemical functionalization contributes to the preparation of more homogenous and soluble material (Fig. 1).

Purification steps involve acidic treatments that lead to the removal of amorphous particles and promote metal oxidation [1]. Aggressive purification procedures can shorten CNTs and produce oxidized nanotubes [2]. On the other hand, a wide variety of functionalization protocols have been reported in the literature [3–5]. In particular, noncovalent strategies, based on van der Waals, hydrophobic, or

*Paper based on a presentation made at the 20th International Conference on Physical Organic Chemistry (ICPOC-20), Busan, Korea, 22–27 August 2010. Other presentations are published in this issue, pp. xxxx–xxxx.

‡Corresponding author

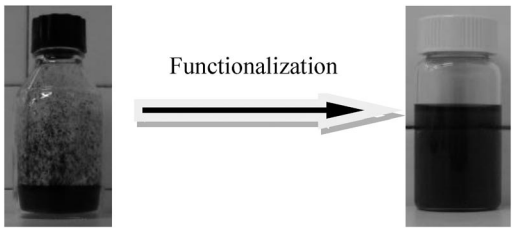

Fig. 1 (left) Powder of pristine MWCNTs, (right) DMF solution of functionalized-MWCNTs after 1,3-dipolar cycloaddition (see Scheme 1).

π–π interactions, are particularly interesting because the electronic structure of CNTs is not perturbed by such "soft" chemistry routes, and they are especially attractive for the surface modification of single-wall carbon nanotubes (SWCNTs). However, for many applications, a network of supramolecular interactions is too weak to implement functional materials. The resulting systems are by far more difficult to control and to characterize than covalent-modified analogues. The extent of functional groups within the supramolecular nano-architecture and their solution stability is often unpredictable and might be exposed to a complicated dynamic evolution. However, noncovalent interactions are reported that use surfactants to exfoliate SWCNT bundles [6], as well as ionic liquids for CNT manipulation and further reactions. CNTs wrapping by polymers, including DNA, have been studied [5]; protein-CNT conjugates have been used for biosensing [7].

The covalent functionalization of CNTs is performed through the introduction of organic moieties by chemical reactions, leading in many cases to the irreversible modification of the nanotube surface, or to a precise tuning of the nano-environment by multiple-step protocols, exploiting reversible processes [8–10]. Reactions can be performed at the nanotube side-wall site (side-wall functionalization) or at the defect sites (defect functionalization), usually localized on the tips. In the first case, fluorination with elemental fluorine at high temperature (400–600 °C) has been explored, accomplishing further substitutions with alkyl groups. Furthermore, radical addition via diazonium salt has been proposed [11]. On the other hand, cycloadditions have been widely applied. Besides 1,3-dipolar cycloadditions of azomethine ylides [12,13], illustrated below, also carbene [2 + 1] or Diels–Alder cycloadditions have been reported, under conventional or microwave (MW)-assisted heating. Side defect functionalization occurs via amidation or esterification reactions of carboxylic residues obtained on CNTs. Moreover, the nanotube terminal caps (i.e., tips when they are not cut) are generally more reactive than side-walls because of their mixed pentagonal–hexagonal structure.

It is noteworthy that while functionalized MWCNTs (f-MWCNTs) do not suffer from a massive perturbation of the inherent electronic properties, and can be implemented upon functionalization, a different behavior is registered for SWCNTs whose extended π-conjugation is perturbed by covalent functionalization and might be irreversibly damaged, preventing the material use for functional applications.

1,3-Dipolar cycloaddition reaction turns out to be one of the most versatile tools to access CNT functionalization for shaping their electronic and physical-chemical properties (Scheme 1).

The reaction employs an α-amino acid and either an aldehyde or a ketone as starting reagents for the in situ generation of a reactive dipolar intermediate, which is able to add to the nanotube double bonds localized both on their side-wall and on their tip. A well-established protocol consists of the addition of an excess of both reactants, in dimethylformamide (DMF), for 5 days at 130 °C. The introduction of protecting-group strategies and MW activation is instrumental for a wide generalization of the synthetic procedure [4,14].

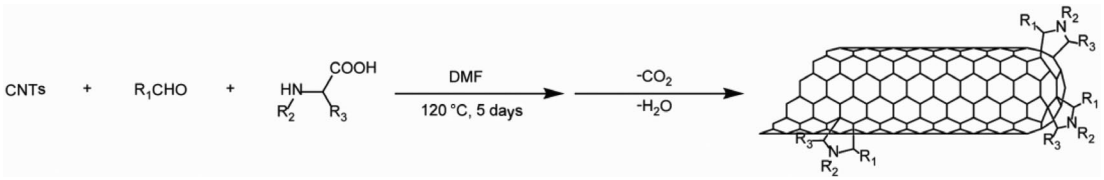

Scheme 1 CNTs addition of azomethine ylides.

We have recently proposed an innovative approach to the multiple decoration of CNTs that avoids any detrimental side effect on their optical and electronic properties, especially in the case of SWCNTs. This is achieved by the introduction of dendronic structures that modify the CNT backbone through the attachment of one focal point carrying multiple pendant functionalities at the periphery [15,16]. By 1,3-dipolar cycloaddition and the divergent growth of a CNT-attached dendron, it is possible to provide the nanotube surface/tips with an increased number of functionalities at the periphery with no major effect on its electronic features.

The advancing generation sequence, leading to a branched dendrimeric unit, is reported in Scheme 2. The successful application of this strategy in shaping the CNT architecture and function is described in the next section dealing with a polyamido-amine (PAMAM) dendritic substituent. For the first proposition of PAMAM dendrimers, see [17].

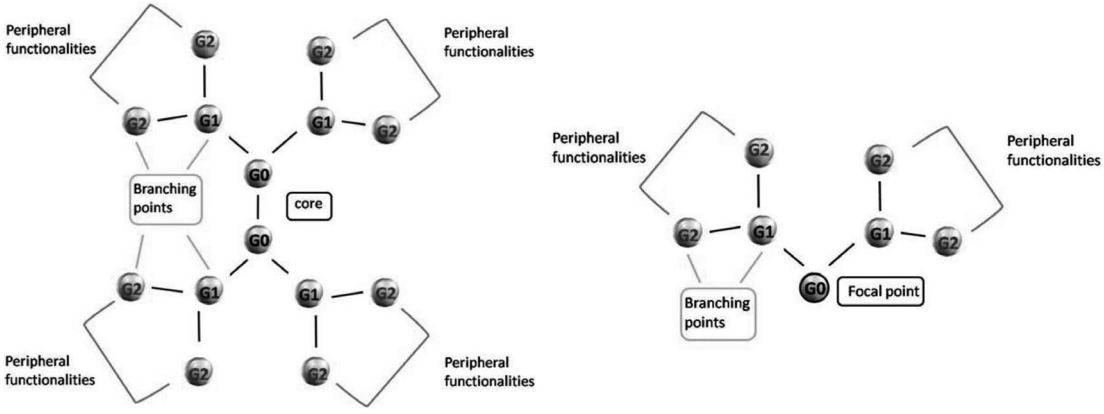

Scheme 2 (left) Dendrimer and (right) dendron structures with generation 0 (G0), generation 1 (G1), and generation 2 (G2).

DENDRON-FUNCTIONALIZED CARBON NANOTUBES

Functionalization of both SWCNTs [15] and MWCNTs [16] with PAMAM dendrons fosters their solubilization in aqueous solution, due to the presence of many polar groups. In both cases, we achieved a second-generation (G2) derivative through a stepwise synthetic process whereby the dendron growth is achieved onto the CNT surface. Pristine CNTs, initially functionalized using 1,3-dipolar cycloaddition of azomethine ylides, underwent a divergent growth of PAMAM dendron and were modified by combining a double addition of methyl acrylate, including a complete addition of the amino groups, with ethylene diamine addition, leading to an exhaustive amidation of the ester functionalities (Scheme 3). The G2 dendron bears the highest number of peripheral primary amino groups (4 amino groups per dendron moiety). At this point, different routes may be envisaged, as the pendant amino substituents are versatile anchoring points. Indeed, we demonstrated the possibility of linking a porphyrin

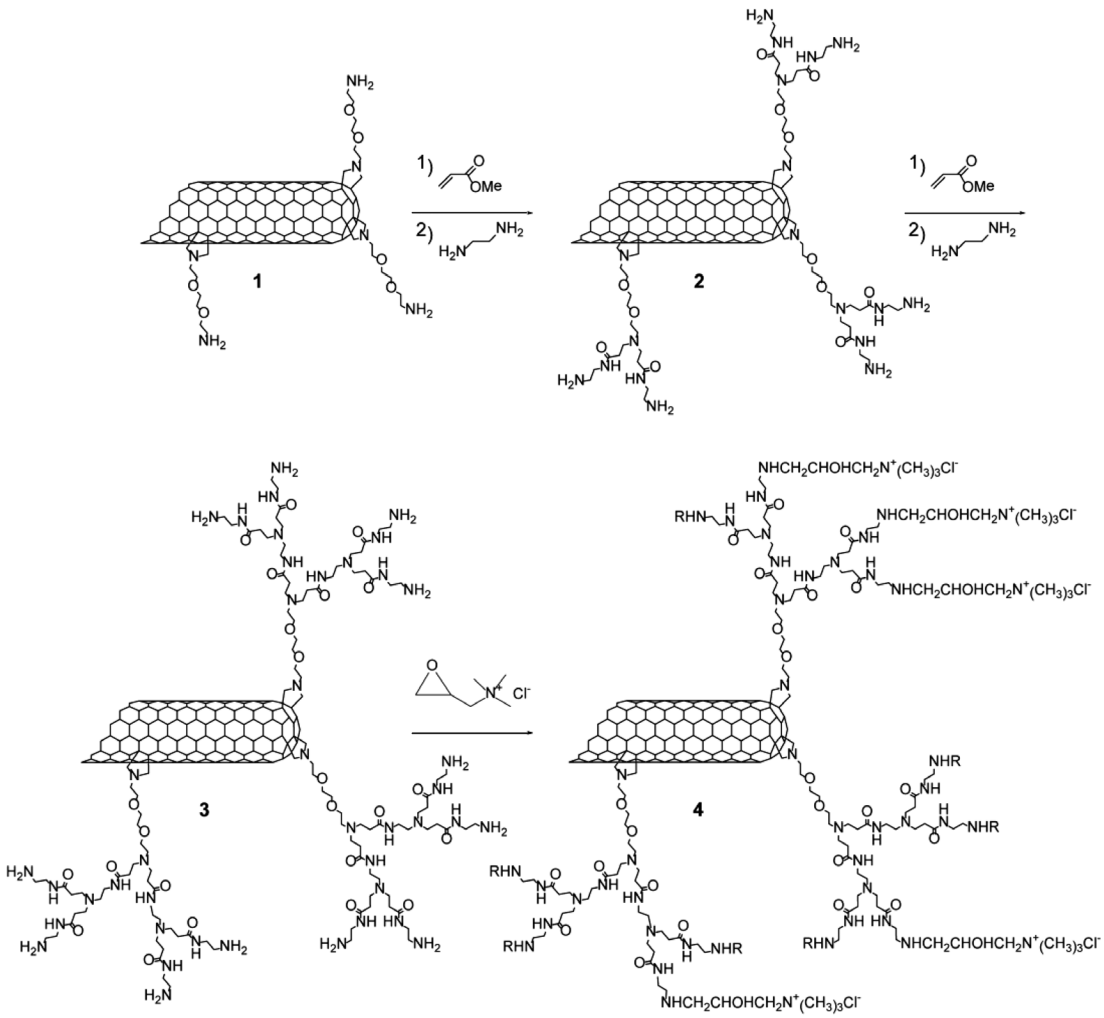

Scheme 3 Reaction conditions for the synthesis of G2 PAMAM dendron-MWCNTs (MeOH, 80 °C, 72 h) and alkylation of primary amino groups with glycidyl trimethylammonium chloride (MeOH, 40 °C, 48 h). R = $–CH_2CH(OH)CH_2N(CH_3)_3{}^+Cl^–$.

derivative enabling photoinduced electron transfer to the SWCNTs scaffolds [15], and in the case of MWCNTs, alkylation using a tailored epoxy derivative yielded polycationic nanotubes (Scheme 3) [18].

In detail, we proceeded in alkylation of (G_2) dendron-MWCNT **3** with a glycidyl trimethylammonium chloride epoxy derivative to generate the highly charged cationic dendron-MWCNT **4** (Scheme 3) [16]. The amount of primary amino groups on MWCNT **1** was measured by the Kaiser test as 0.481 mmol/g. Subsequent Kaiser tests gave amine loadings of 0.718 and 1.097 mmol/g for the G1 and G2 dendrimers, respectively. The test gave negative results for the alkylated conjugate **4**, consistent with complete conversion of the primary amino groups.

The different CNT derivatives were fully characterized by standard techniques, such as thermogravimetric analysis (TGA) and transmission electron microscopy (TEM). Figure 2 displays the dispersibility of MWCNTs evaluated by means of TEM.

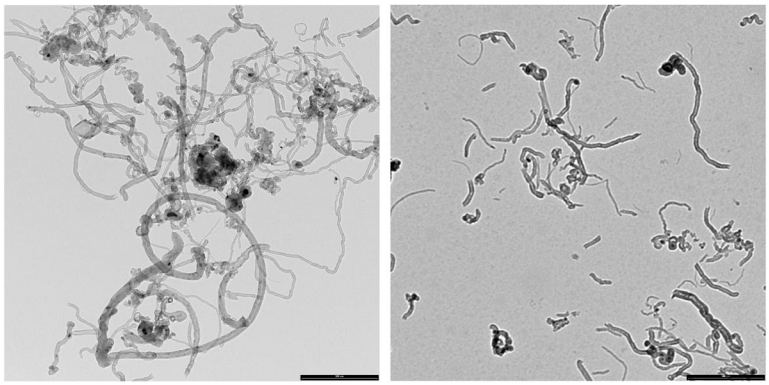

Fig. 2. TEM image of (left) MWCNT **1**; (right) dendron-MWCNT **4**. Scale bar is 500 nm.

The weight loss measured by TGA was correlated to the mass increase of the functionalized CNT (Fig. 3). The number of the functional groups for dendron-MWCNT **4** calculated from the TGA curve corresponds to 0.237 mmol/g, resulting in 0.948 mmol/g of amine groups for the precursor MWCNT **3**. This value was in good agreement with the Kaiser test results (1.097 mmol/g).

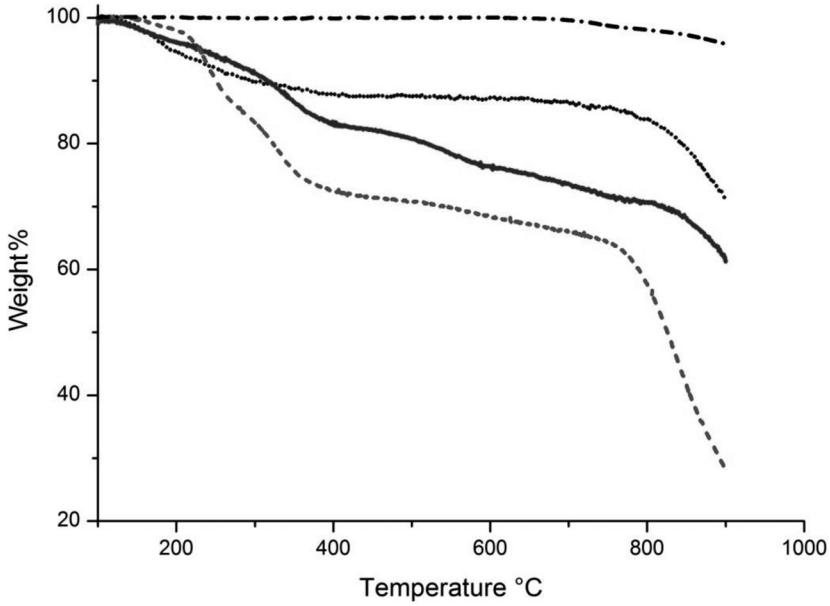

Fig. 3 TGA curves of pristine MWCNTs (dash dot line), G1 dendron-MWCNT **2** (dot line), G2 dendron-MWCNTs **3** (solid line), and alkylated G2 dendron-MWCNT **4** (dash line). All the experiments were performed under N_2 atmosphere.

FUNCTIONALIZED CARBON NANOTUBES BEARING MULTIPLE POSITIVE-CHARGES AND DECORATION WITH WATER-SPLITTING POLYOXOMETALATES

Thanks to the introduction of resident positive charges, f-MWCNT **4** can serve to efficiently scavenge polyanions via electrostatic interactions. For instance, it was possible to anchor toxic-siRNA (small

interference RNA) sequences, in the field of drug delivery [16,19]. Recently, the same approach has been successfully applied to decorate f-MWCNT **4** with catalytic metal-oxide clusters, belonging to the family of polyoxometalates (POMs) [20]. POMs are discrete, soluble anionic aggregates of early transition metals and oxygen. These molecular multiple metal-oxo clusters are characterized by a rich variety of structures, having different chemical composition, charge, and counter ions, and they show noticeable applications in the field of catalysis and functional materials [21]. Especially, the possibility of including redox active multi-transition metals (like Mn, Co, or Ru) within a highly robust, water-soluble, inorganic scaffold, with enhanced electron-acceptor and proton exchange properties, makes them an attractive molecular alternative to IrO_2 or RuO_2 colloidal catalysts for water oxidation.

Indeed, water oxidation to dioxygen is recognized as the rate-limiting step of artificial photosynthesis, i.e., the light-driven water splitting into hydrogen and oxygen. This is related to the mechanistic complexity of the process, which involves removal of 4 electrons and 4 protons from water and the formation of a new oxygen–oxygen bond [22]. Moreover, the harsh oxidizing conditions employed to achieve water oxidation usually hamper the long-term stability of metal catalysts based on organic ligands.

A recent breakthrough in the field is the discovery of a tetraruthenium-substituted POM with oxygenic activity, mimicking the photosynthesis natural enzyme [23–25].

The solid-state structure of $[Ru^{IV}_4(\mu\text{-}O)_4(\mu\text{-}OH)_2(H_2O)_4(\gamma\text{-}SiW_{10}O_{36})_2]^{10-}$, hereafter **$Ru_4$POM**, is shown in Fig. 4, and features a tetraruthenate adamantane-like core embedded by two $\gamma\text{-}SiW_{10}O_{36}^{8-}$ polyoxometalate units. The four ruthenium centers are indeed connected through μ-oxo or μ-hydroxo bridges, and resemble the connectivity of the four manganese atoms in the oxygen-evolving center of the photosystem II enzyme [26–28]. Water oxidation catalyzed by **Ru_4POM** is observed in homogeneous aqueous solution, in the presence of sacrificial [23,24] or photogenerated [29] oxidants, with outstanding activity, robustness, and unprecedented quantum yields when combined with ruthenium polypyridine photosensitizers.

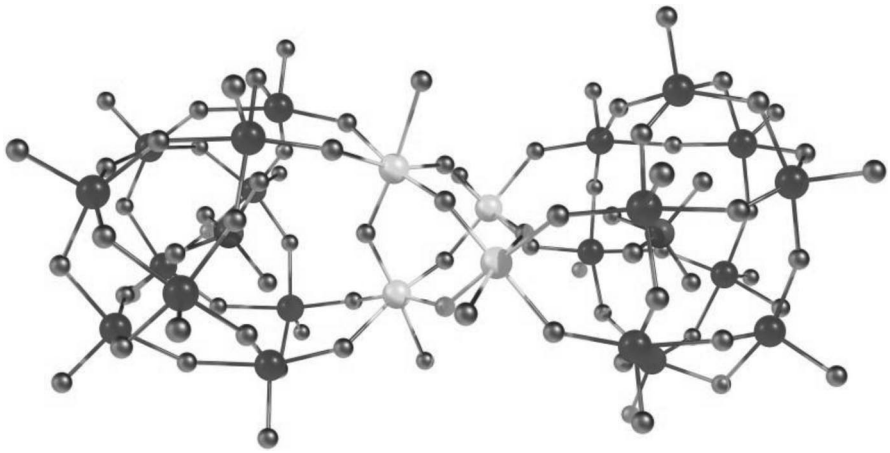

Fig. 4 Structure of $[Ru^{IV}_4(\mu\text{-}O)_4(\mu\text{-}OH)_2(H_2O)_4(\gamma\text{-}SiW_{10}O_{36})_2]^{10-}$ [23].

These observations offer great premises for the assembly of a photoelectrolysis cell integrating nanostructured anodes based on molecular POMs. The construction of a doped oxygen-evolving anode (OEA), responsible for the electron/proton flux feeding the reductive end for water splitting and generating hydrogen represents a major goal for renewable energy applications.

Toward this aim, the fabrication of hybrid CNTs has been envisaged, using the PAMAM-modified MWCNTs to anchor **Ru_4POM** on their surface.

The resulting material is thus assembled by means of electrostatic interactions between the organic and inorganic domains, and it has been used for the fabrication of novel OEA as detailed in the next paragraph. The efficiency of the OEA, its operative voltage, current density, and operation stability are pivotal features for a viable hydrogen economy, being the focus of the current research effort in this area. We have shown that fast and continuous O_2 evolution is achieved at the heterogeneous surface of indium tin oxide (ITO) electrodes upon deposition of the hybrid CNTs integrating the **Ru_4POM** domains (Fig. 5). The interplay of the bio-inspired catalytic domains with the carbon nanostructures is instrumental for electrocatalytic O_2 generation at low overpotential (<0.35 V), and with multi-cycling performance.

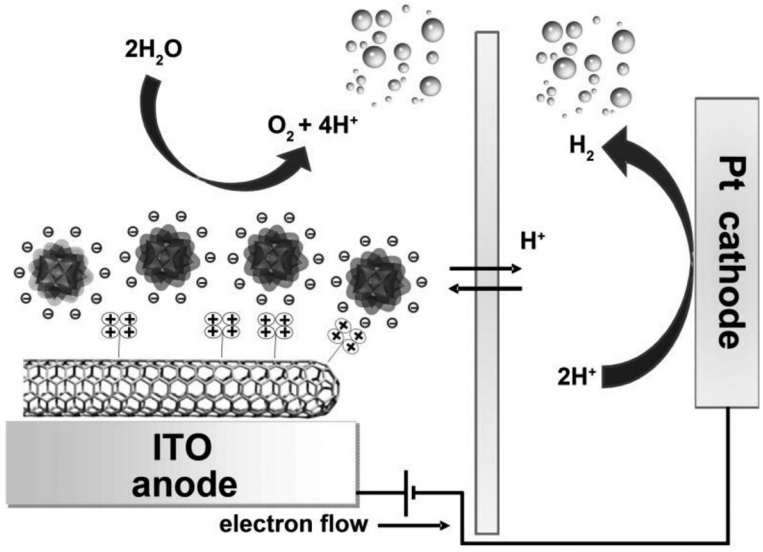

Fig. 5 Schematic sketch of the cell for water electrolysis.

RuPOM@DENDRON-FUNCTIONALIZED CARBON NANOTUBES: SYNTHESIS AND CHARACTERIZATION

Straightforward metathesis techniques in water solution were adopted to anchor the catalytically active **Ru_4POM** to the positively charged PAMAM-modified MWCNTs **4** (Scheme 4). Specifically, different amounts (0.4–1.6 mmol) of the lithium salt of the catalyst, $Li_{10}[Ru_4(\mu\text{-}O)_4(\mu\text{-}OH)_2(H_2O)_4(\gamma\text{-}SiW_{10}O_{36})_2]$, ($Li_{10}$ **Ru_4POM**) were dissolved in water (pH = 5) and left overnight under stirring in the presence of MWCNTs **4** (5 mg), as shown in Scheme 4. The resulting hybrid products **Ru_4POM@MWCNTs** were recovered through filtration and extensively washed with water. The TGA under air profiles (Fig. 6) allow the calculation of the catalyst loading on CNTs.

Increasing **Ru_4POM** amounts were used in order to optimize the catalyst loading onto the CNTs. Optimal conditions were achieved by using 1.6 mmol of **Ru_4POM**; higher amounts of **Ru_4POM** did not produce further significant improvement in the final loading, probably as a consequence of saturation of the positive charges of the modified MWCNTs. As expected, only a negligible POM loading is observed when exposed to non-(positively) charged CNTs, thus highlighting the fundamental role played by the PAMAM functional groups in driving and directing the POM anchoring on the carbon surface.

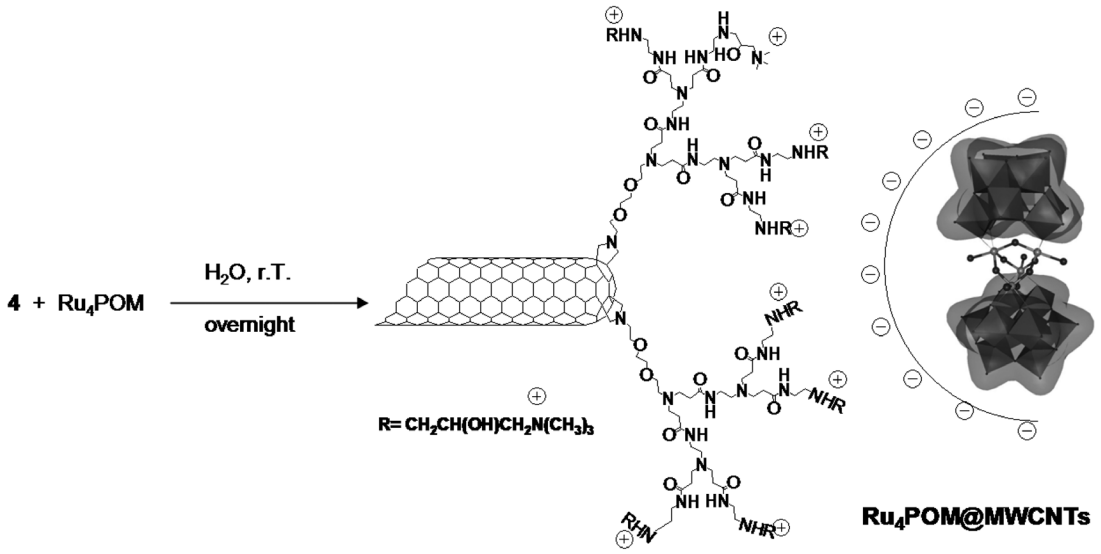

Scheme 4 MWCNTs **4** Li_{10}RuPOM ion metathesis in which **Ru_4POM@MWCNTs** has been formed.

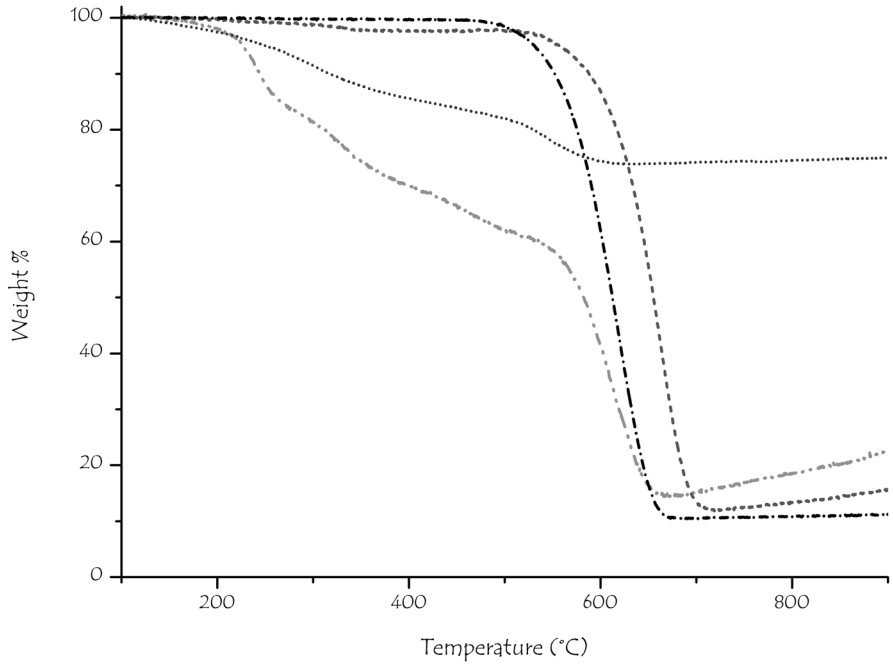

Fig. 6 TGA under air of MWCNTs as produced (dash dot line), MWCNTs **4** (dash dot dot line), **Ru_4POM@MWCNTs** (dot line), and non-charged Ru_4POM@MWCNTs (dash line).

The **Ru_4POM** complex on the CNT surface maintains the solid-state structure, as clearly demonstated by Raman spectra collected for sample **Ru_4POM@MWCNTs** (Fig. 7).

In Raman spectra, **Ru_4POM** bands are visible in the region 500–900 cm^{-1} [25], while the CNT features are observed at 1350–2720 cm^{-1} (Fig. 7). In particular, the O–Ru–O asymmetric stretching

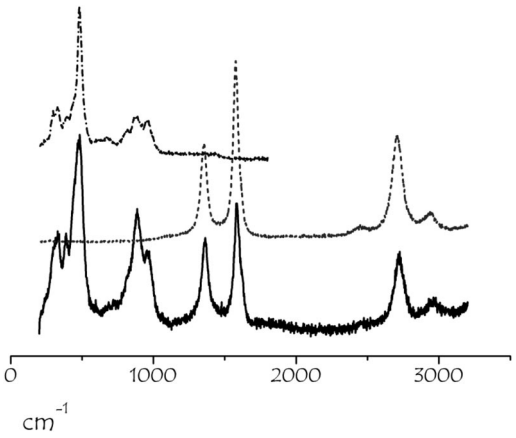

Fig. 7 Raman spectra of **Ru_4POM@MWCNTs** (solid), non-charged Ru_4POM@MWCNTs (dash line), **Ru_4POM** (dash dot line).

band is distinguishable at ca. 500 cm^{-1}, whereas the asymmetric stretching of O–W–O is around 900 cm^{-1}. MWCNTs bear their characteristic D band, G band, and G' band at 1350, 1600, and 2720 cm^{-1}, respectively. As expected, no characteristic peaks of **Ru_4POM** are present in material recovered using the non-charged MWCNTs.

TEM images show the presence of metal-centered domains ascribed to **Ru_4POMs** on the CNTs surface (Fig. 8), this especially evident when compared to TEM images of MWCNTs **4** and pristine materials.

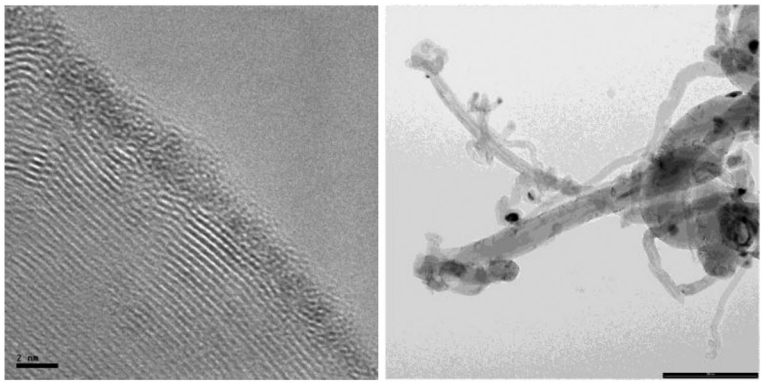

Fig. 8 (left) High-resolution TEM image of derivative **Ru_4POM@MWCNTs** (scale bar 2 nm) and (right) TEM image of non-charged MWCNTs recovered after reaction with **Ru_4POM** (scale bar: 100 nm).

Ru_4POM@CARBON NANOSTRUCTURES: ELECTROCATALYSIS

One of the most useful advantages of nanostructured materials for electrocatalytic application is the increase of surface area, and interfacial contact. Furthermore, the 1D morphology of CNTs and their peculiar electron conductivity might leverage significant improvement promoting electron-transfer processes. This latter aspect has been addressed by repeating the functionalization/decoration steps described above, using AC as scaffold. To this purpose, AC was reacted to obtain a positively charged PAMAM-modified derivative, to be coupled with **Ru_4POM** (Scheme 5).

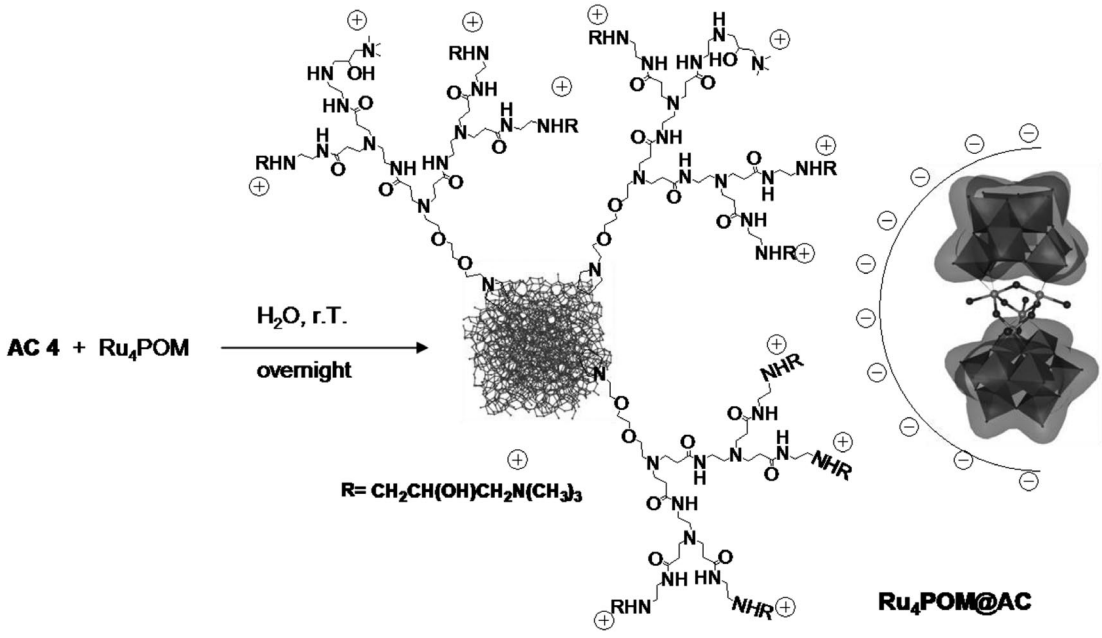

Scheme 5 Representation of **Ru_4POM@AC** preparation.

The AC derivatives were characterized by means of TGA and TEM (Fig. 9).

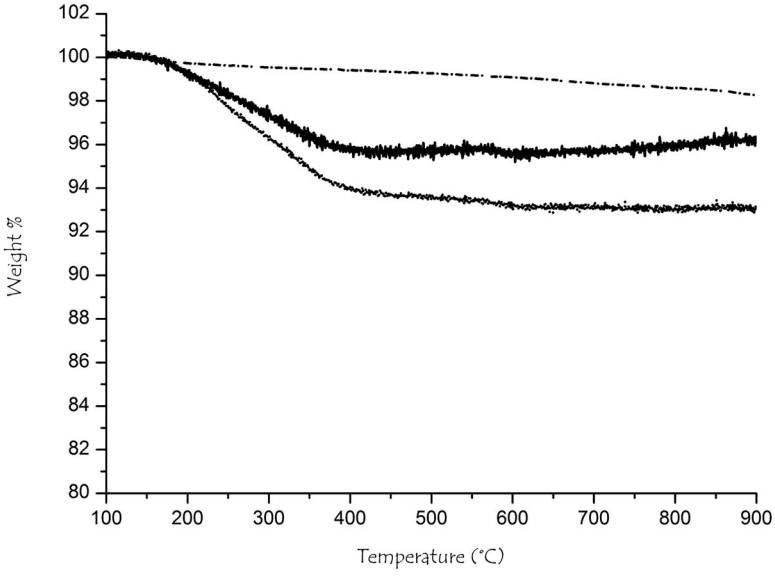

Fig. 9 TGA (under N_2) curves of pristine AC (dash dot line) and of AC **3** (solid line) and AC **4** (dot line).

For both compounds AC **3** and **4** bearing, respectively, the Dendron (AC **3**) and the polycationic Dendron (AC **4**), the functional groups calculated by means of TGA under N_2 are 0.040 mmol/g (with a theoretical amount of amino groups in AC **3** of 0.160 mmol/g), so a bit lower with respect to MWCNTs derivatives. The Kaiser test result for AC **3** was 0.120 mmol/g, and this result is quite similar to the one obtained with TGA (Fig. 10).

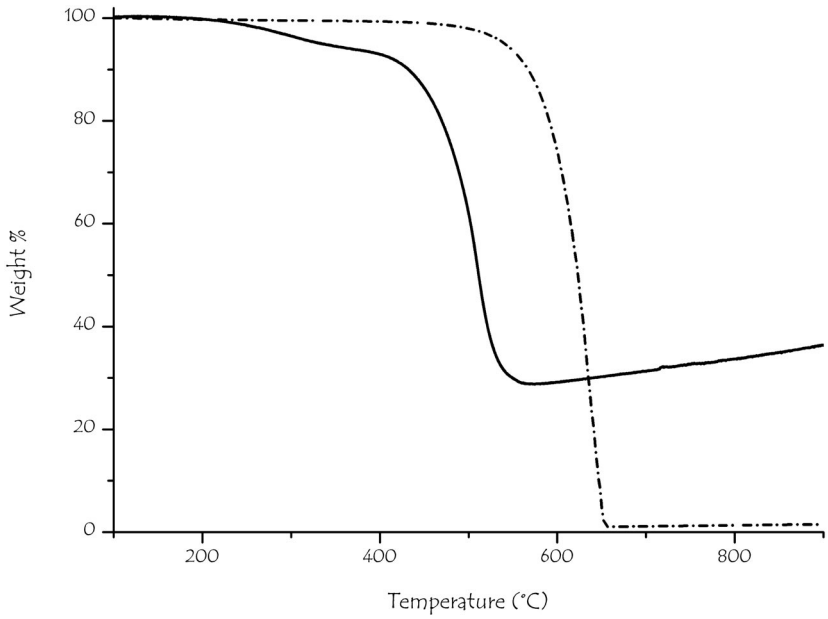

Fig. 10 TGA (under air) curves of AC (dash dot line) and of **Ru_4POM@AC** (solid line).

The loading of **Ru_4POM** on PAMAM-modified AC turns out to be 0.6 mmol/g. In TEM images (Fig. 11), a deeper contrast for the **Ru_4POM@AC** derivative could represent **Ru_4POM** domains on the AC nanoparticles.

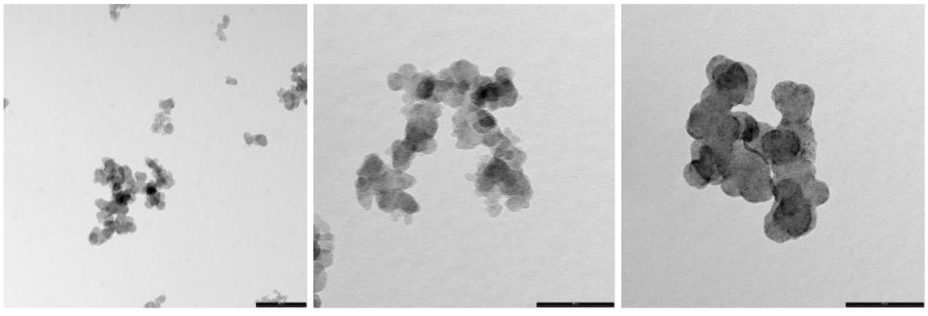

Fig. 11 TEM images of: (left) AC as pristine (scale bar 200 nm), (center) AC **4** (scale bar 100 nm); (right) **Ru_4POM@AC** (scale bar 100 nm).

OEAs integrating **Ru_4POM@MWCNTs** and **Ru_4POM@AC** were obtained upon drop-casting the hybrid nanocomposites as a water solution on ITO electrodes (3 × 3 mm). Analysis of the resulting

coating by X-ray photoelectron spectroscopy (XPS) reveals the expected peaks assigned to the W(VI) component of the POM framework, and to a Ru 3d peak attributed to high-valent states. Scanning electron microscopy (SEM) images of the **Ru_4POM@MWCNTs** electrode show a highly porous 3D extended network, built from interconnecting CNTs carrying the inorganic catalyst (Fig. 12, left). SEM evidence collected for the **Ru_4POM@AC** electrode confirms the deposition of porous film displaying a globular matrix (Fig. 12, right). The hybrid materials possess high surface area and nanosized domains with enhanced hydrophilic character, due to the contemporary presence of W/Ru sites and the charged nitrogen/oxygen residues. Such an environment is therefore chemically tailored to assist water diffusion and stabilization through coordination and H-bonding interactions. AFM measurements provide direct evidence of the film roughness, which is associated with the effective surface area of the system. The root mean square (rms) roughness value, evaluated on the reported 10 × 10 μm area, is 150 nm, which is notably higher than a flat silica sample, generally characterized by a rms ~1 nm.

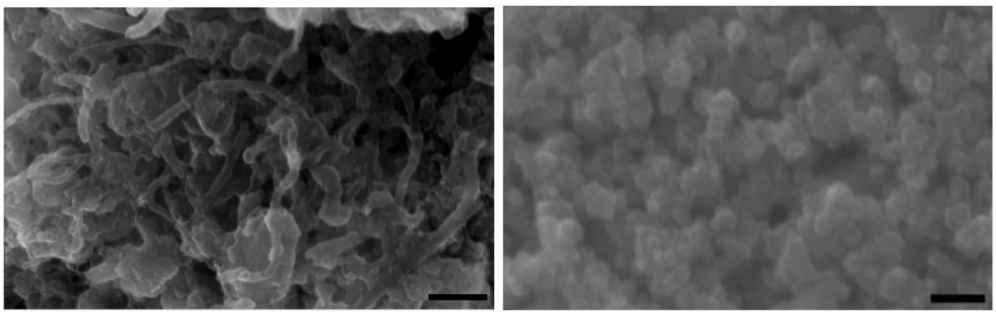

Fig. 12 SEM images of a highly porous **Ru_4POM@MWCNT** film (left, scale bar 100 nm) the **Ru_4POM@AC** (right, scale bar 100 nm) on ITO.

The electrocatalytic performance of both **Ru_4POM@MWCNTs** and **Ru_4POM@AC** deposited on ITO substrates has been evaluated vis-à-vis the oxygen evolving activity upon electrocatalytic water oxidation. The close similarity of the morphology and surface properties for both composites allows the electrocatalytic performance to be ascribed to the intrinsic features of the nanostructured carbon-based matrix under examination.

The catalytic activity of the modified ITO electrodes was studied by cyclic voltammetry in a standard three-electrode cell, equipped with an Ag/AgCl reference electrode and a Pt wire counter electrode, containing an aqueous solution at pH = 7 (PBS buffer), in air and at room temperature (Fig. 13). As expected, the POM-free MWCNT **4** is catalytically inert (Fig. 13). By contrast, ITO electrodes doped with **Ru_4POM** exhibit in all cases an oxidation wave at 0.9 V followed by the onset of a catalytic wave at applied voltages >1.10 V, due to water oxidation. With respect to oxygen production, the relative electrocatalytic activity of the catalyst on ITO surface strongly depends on its environment and stands in the order **Ru_4POM < Ru_4POM@AC << Ru_4POM@MWCNTs** (compare curves in Fig. 13).

The superior performance of the nanostructured electrode is likely due to a synergistic interplay of factors, coupling the redox features of **Ru_4POM** with the MWCNT-enabled electrical wiring of the hybrid material. Indeed, turnover frequency (TOF, i.e., the turnover number related to oxygen generation per unit time), values in the range 36–306 h^{-1} were achieved depending on the applied overpotential. At pH = 7.0, an appreciable catalytic current with a remarkable TOF (36 h^{-1}) is observed beginning at η = 0.35 V, and reaching a peak performance of 306 h^{-1} at η = 0.60 V. The TOF efficiency exceeds the values previously reported for Co- or Mn-based systems, found in the range 0.7–20 h^{-1} at $\eta \geq 0.40$ V [30–32]. While homogeneous studies of water splitting have demonstrated the advantage of

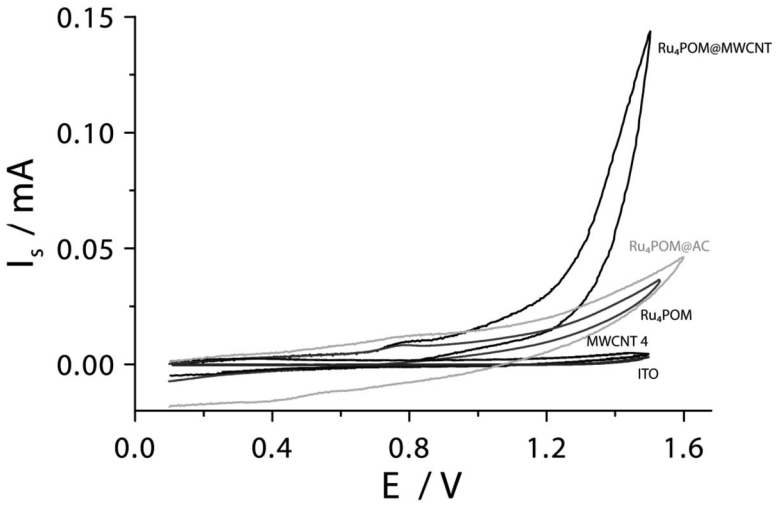

Fig. 13 Cyclic voltammetric (CV) curves of ITO deposited **Ru_4POM@MWCNT**, **Ru_4POM@AC**, **Ru_4POM**, **MWCNT 4**, and bare **ITO** at pH = 7.

storing multiple redox equivalents in a single catalyst [33], our results address the importance of hybrid interfaces/contacts to control and promote electron-transfer events at heterogeneous surfaces.

CONCLUSION

In conclusion, the functionalization of CNTs via covalent chemistry leads to the introduction of pendant groups and dendrimeric structures to serve as interface with functional molecules, and retaining an unprecedented potential for drug delivery and catalysis. Our use of tailored and functionalized MWCNTs implements the design of water-splitting electrodes, whose efficiency, operative voltage, current density, and operational stability represent a definite step forward in the direction of a viable hydrogen economy. Optimization of this system and cost prospects are currently under evaluation.

ACKNOWLEDGMENTS

This work was financially supported by the University of Trieste, INSTM, Italian Ministry of Education MIUR (cofin Prot. 20085M27SS and Firb RBIN04HC3S), the University of Padova (Progetto Strategico 2008, HELIOS, prot. STPD08RCX) and Fondazione Cariparo (Nano-Mode, progetti di eccellenza 2010). We are very grateful to Prof. Francesco Paolucci and Dr. Chiara Maccato for their great collaborative work.

REFERENCES

1. J. Liu. *Science* **280**, 1253 (1998).
2. K. J. Ziegler, Z. Gu, H. Peng, E. L. Flor, R. H. Hauge, R. E. Smalley. *J. Am. Chem. Soc.* **127**, 1541 (2005).
3. A. Hirsch. *Angew. Chem., Int. Ed.* **41**, 1853 (2002).
4. P. Singh, S. Campidelli, S. Giordani, D. Bonifazi, A. Bianco, M. Prato. *Chem. Soc. Rev.* **38**, 2214 (2009).
5. D. Tasis, N. Tagmatarchis, A. Bianco, M. Prato. *Chem. Rev.* **106**, 1105 (2006).
6. L. Vaisman, H. Wagner, G. Marom. *Adv. Colloid Interface Sci.* **128–130**, 37 (2006).

7. A. Jorio, G. Dresselhaus, M. S. Dresselhaus. *Carbon Nanotubes: Advanced Topics in the Synthesis, Structure, Properties and Applications*, 1st ed., Springer, Heidelberg (2008).
8. A. Hirsch. *Nat. Mater.* **9**, 868 (2010).
9. I. Guryanov, F. M. Toma, A. Montellano Lopez, M. Carraro, T. Da Ros, G. Angelini, E. D'Aurizio, A. Fontana, M. Maggini, M. Prato, M. Bonchio. *Chem.—Eur. J.* **15**, 12837 (2009).
10. M. Prato. *Nature* **465**, 172 (2010).
11. J. L. Bahr, J. Yang, D. V. Kosynkin, M. J. Bronikowski, R. E. Smalley, J. M. Tour. *J. Am. Chem. Soc.* **123**, 6536 (2001).
12. V. Georgakilas, K. Kordatos, M. Prato, D. M. Guldi, M. Holzinger, A. Hirsch. *J. Am. Chem. Soc.* **124**, 760 (2002).
13. V. Georgakilas, N. Tagmatarchis, D. Pantarotto, A. Bianco, J. Briand, M. Prato. *Chem. Commun.* **24**, 3050 (2002).
14. E. Vázquez, M. Prato. *Pure Appl. Chem.* **82**, 853 (2010).
15. S. Campidelli, C. Sooambar, E. Diz, C. Ehli, D. Guldi, M. Prato. *J. Am. Chem. Soc.* **128**, 12544 (2006).
16. M. A. Herrero, F. M. Toma, K. T. Al-Jamal, K. Kostarelos, A. Bianco, T. Da Ros, F. Bano, L. Casalis, G. Scoles, M. Prato. *J. Am. Chem. Soc.* **131**, 9843 (2009).
17. D. A. Tomalia, H. Baker, J. Dewald, M. Hall, G. Kallos, S. Martin, J. Roeck, J. Ryder, P. Smith. *Polym. J.* **17**, 117 (1984).
18. S. Oh, Y. Kim, H. Ye, R. M. Crooks. *Langmuir* **19**, 10420 (2003).
19. K. T. Al-Jamal, F. M. Toma, A. Yilmazer, H. Ali-Boucetta, A. Nunes, M. A. Herrero, B. Tian, A. Eddaoui, W. T. Al-Jamal, A. Bianco, M. Prato, K. Kostarelos. *FASEB J.* **24**, 4354 (2010).
20. F. M. Toma, A. Sartorel, M. Iurlo, M. Carraro, P. Parisse, C. Maccato, S. Rapino, B. Rodriguez Gonzalez, H. Amenitsch, T. Da Ros, L. Casalis, A. Goldoni, M. Marcaccio, G. Scorrano, G. Scoles, F. Paolucci, M. Prato, M. Bonchio. *Nat. Chem.* **2**, 826 (2010).
21. E. Coronado, C. J. Gomez-Garcia. *Chem. Rev.* **98**, 273 (1998).
22. I. Romero, M. Rodríguez, C. Sens, J. Mola, M. L. Kollipara, L. Francás, E. Mas-Marza, L. Escriche, A. Lloblet. *Inorg. Chem.* **47**, 1824 (2008).
23. A. Sartorel, M. Carraro, G. Scorrano, R. De Zorzi, S. Geremia, N. D. McDaniel, S. Bernhard, M. Bonchio. *J. Am. Chem. Soc.* **130**, 5006 (2008).
24. Y. Geletii, B. Botar, P. Kögerler, D. Hillesheim, D. Musaev, C. Hill. *Angew. Chem., Int. Ed.* **47**, 3896 (2008).
25. A. Sartorel, P. Miró, E. Salvadori, S. Romain, M. Carraro, G. Scorraro, M. Di Valentin, A. Lloblet, C. Bo, M. Bonchio. *J. Am. Chem. Soc.* **131**, 16051 (2009).
26. B. Loll, J. Kern, W. Saenger, A. Zouni, J. Biesiadka. *Nature* **438**, 1040 (2005).
27. K. N. Ferreira, T. M. Iverson, K. Maghlaoui, J. Barber, S. Iwata. *Science* **303**, 1831 (2004).
28. J. Yano, J. Kern, K. Sauer, M. J. Latimer, Y. Pushkar, J. Biesiadka, B. Loll, W. Saenger, J. Messinger, A. Zouni, V. K. Yachandra. *Science* **314**, 821 (2006).
29. F. Puntoriero, G. La Ganga, A. Sartorel, M. Carraro, G. Scorrano, M. Bonchio, S. Campagna. *Chem. Commun.* **46**, 4725 (2010).
30. M. W. Kanan, D. G. Nocera. *Science* **321**, 1072 (2008).
31. R. Brimblecombe, G. Swiegers, G. Dismukes, L. Spiccia. *Angew. Chem., Int. Ed.* **47**, 7335 (2008).
32. R. Brimblecombe, D. Kolling, A. Bond, G. Dismukes, G. Swiegers, L. Spiccia. *Inorg. Chem.* **48**, 7269 (2009).
33. L. Tinker, N. McDaniel, S. Bernhard. *J. Mater. Chem.* **19**, 3328 (2009).

